1H, 13C and 15N resonance assignments of the RodA hydrophobin from the opportunistic pathogen Aspergillus fumigatus

Ariane Pille, Ann H. Kwan, Ivan Cheung, Matthew Hampsey, Vishukumar Aimanianda, Muriel Delepierre, Jean-Paul Latgé, Margaret Sunde, J. Iñaki Guijarro

^{1}H, ^{13}C and ^{15}N resonance assignments of the RodA hydrophobin from the opportunistic pathogen *Aspergillus fumigatus*

Ariane Pille • Ann H. Kwan • Ivan Cheung • Matthew Hampsey • Vishukumar Aimanianda • Muriel Delepierre • Jean-Paul Latgé • Margaret Sunde • J. Iñaki Guijarro

Ariane Pille • Muriel Delepierre • J. Iñaki Guijarro
Institut Pasteur, Unité de RMN des Biomolécules, Dépt. Biologie Structurale et Chimie, 25 rue Du Dr. Roux 75015 Paris, France
CNRS UMR 3528, 75015 Paris, France

Ariane Pille
Sorbonne Universités, UPMC Univ Paris 06, IFD, 4 Place Jussieu, 75252 Paris cedex 05, France

Ann H. Kwan • Ivan Cheung • Matthew Hampsey
School of Molecular Bioscience, University of Sydney, NSW 2006 Sydney, Australia

Margaret Sunde
School of Medical Sciences, University of Sydney, NSW 2006 Sydney, Australia

Vishukumar Aimanianda • Jean-Paul Latgé
Institut Pasteur, Unité des Aspergillus, Dépt de Parasitologie et Mycologie, 28 rue Du Dr. Roux, 75015 Paris, France

Correspondence to:

J. Iñaki Guijarro
E-mail: inaki.guijarro@pasteur.fr, tel: +(33)144389398, fax: +(33)145688940

keywords: hydrophobin, functional amyloids, rodlets, cell wall, *Aspergillus fumigatus*, NMR

Abstract Hydrophobins are fungal proteins characterised by their amphipathic properties and an idiosyncratic pattern of eight cysteine residues involved in four disulphide bridges. The soluble form of these proteins spontaneously self-assembles at hydrophobic/hydrophilic interfaces to form an amphipathic monolayer. The RodA hydrophobin of the opportunistic pathogen *Aspergillus fumigatus* forms an amyloid layer with a rodlet morphology that covers the surface of fungal spores. This rodlet layer bestows hydrophobicity to the spores facilitating their dispersal in the air and rendering the conidia inert relative to the human immune system. As a first step in the analysis of the solution structure and self-association of RodA, we report the ^{1}H, ^{13}C and ^{15}N resonance assignments of the soluble monomeric form of RodA.

Biological context

Hydrophobins are small (< 20 kDa) amphipathic proteins produced by most filamentous fungi. These proteins with remarkable physicochemical properties are defined by a pattern of eight cysteine (Cys) residues that form four disulphide bonds (C1−C6, C2−C5, C3−C4, C7−C8) (Kwan *et al.* 2006). They are produced in a soluble form that spontaneously self-assembles at hydrophobic/hydrophilic or air/water interfaces to form amphipathic monolayers with high surfactant activity. Hydrophobins are divided in two classes based on their sequence, hydropathy and on the physicochemical characteristics of the monolayers (Wosten *et al.* 1994). Class I hydrophobins show very little conservation in their amino acid sequence and vary in size, with different spacings between cysteine residues; these hydrophobins associate into very robust monolayers that are resistant to detergents even at boiling temperatures and require concentrated acids to dissociate. Class I hydrophobin monolayers show a very well ordered rodlet morphology and display the hallmarks of amyloid fibres (Wosten and de Vocht 2000). The amino acid sequences of class II hydrophobins are more conserved, they show less size and inter-cysteine-spacing variability; the corresponding monolayers do not contain amyloid fibres and can be disaggregated with detergents and hot alcohol solutions. Although some degree of order has been observed for hydrophobins HFBI (Szilvay *et al.* 2007) and NC2 monolayers (Ren *et al.* 2013a), class II hydrophobins seem to form less well ordered monolayers. The structures of the soluble forms of hydrophobins from both classes that self-associate into monolayers are quite different but show a common central β-barrel stabilised by the four disulphide bridges and surrounding loops of different length and secondary structure (Sunde *et al.* 2008). The biological functions of hydrophobins rely on the formation of the amphipathic monolayers. Hydrophobins are used by fungi to breach the air/water barrier and develop aerial hyphae by lowering the surface tension of the aqueous environment, to prevent water-logging, to facilitate aerial growth and spore dispersion, to participate in the extracellular matrix and biofilms as well as to form a protective layer during fruiting body development. Hydrophobins can also participate in host-fungi interactions and have been described as pathogenicity factors in plant- or entomo-pathogenic fungi. The surfactant activity of hydrophobins and the capacity to reverse the wettability of surfaces offers the possibility to use these proteins for different biotechnological applications such as drug delivery, cell attachment, surface functional modification and protein purification. The biological functions, structural knowledge and biotechnical applications of hydrophobins have been reviewed in

(Wosten 2001;Scholtmeijer *et al.* 2001;Tucker and Talbot 2001;Linder *et al.* 2005;Bayry *et al.* 2012;Ren *et al.* 2013b).

Aspergillus fumigatus is an opportunistic pathogen than can cause a variety of diseases in immunocompromised individuals that range from allergies to threatful invasive aspergillosis. This filamentous fungus has become the major aerial fungal pathogen of humans and represents a major burden in terms of morbidity, mortality and cost for hospitals (Hayes and Denning 2013). The conidia, which are the infective form of the fungus, are covered by a rodlet layer formed by the class I hydrophobin RodA (Paris *et al.* 2003). This proteinaceous coat bestows hydrophobicity to the spores facilitating their dispersal in the air and masks pathogen-associated molecular patterns (PAMPs) thus rendering the conidia inert relative to the innate and adaptive immune systems (Aimanianda *et al.* 2009). With the aim of understanding the mechanism of rodlet formation and the rodlet structure, as well as shedding light on the possible links between the structure of RodA and its immunologic characteristics, we are analysing the solution structure of RodA, its self-assembly, the structure of the rodlets and the immunological characteristics of RodA mutants. Here we describe the ^{1}H, ^{15}N, ^{13}C resonance assignments of the soluble form of RodA and the comparison of its secondary structure and dynamics with that of other hydrophobins.

Materials and Methods

Protein Preparation

The RodA gene sequence (AAB07707) was cloned into a pHUE expression vector used for other hydrophobins (Kwan *et al.* 2006) to generate the plasmid pHUE-RodA. The resulting plasmid encodes for a fusion protein (H_6-Ub-RodA) of N-terminal hexa-histidine-tagged ubiquitin (H_6-Ub) coupled to RodA and contains a deubiquinating UBP41 enzyme cleavage site between the ubiquitin and RodA proteins. The plasmid also codes for ampicillin resistance.

The protein H_6-Ub-RodA was expressed using the *Escherichia coli* BL21 (DE3) strain. Bacteria were grown at 37°C in minimal M9 media supplemented with 0.43 g/L of yeast extract without amino acids and without ammonium sulphate (DIFCO), and containing $^{15}NH_4Cl$ (0.52 g/L, ≥ 98%) and $^{13}C_6$ glucose (2 g/L, ≥ 98%) as sole sources of nitrogen and carbon, respectively. When cultures reached an absorbance of 0.6 at 600 nm, expression was induced with 0.5 mM isopropyl-β-thio-galactopyranoside. Cells were harvested by centrifugation at 6700 g and 4°C after three hours of induction, resuspended in 150 mM Tris-HCl, 300 mM NaCl pH 8, re-pelleted by centrifugation and frozen at -80°C.

The fusion protein was obtained simultaneously from both the soluble and insoluble fractions under denaturing and reducing conditions, purified by affinity chromatography and folded under oxidative conditions. To extract the protein, the cell pellet was thawed and solubilised with buffer A (10 mM TrisHCl, 100 mM NaH_2PO_4, 4 mM β-mercaptoethanol [βME], 8 M urea pH 8). After eliminating the cell debris by centrifugation, H_6-Ub-RodA was loaded into a nickel column (Hitrap™, GE Healthcare) pre-equilibrated with buffer A. The column was successively washed with the equilibrating buffer prepared at pH 8 and at pH 6.3. The fusion protein was then eluted with the same buffer prepared at pH 4.3. Oxidative refolding was performed by dialysis of the eluted protein at 4°C against

the refolding buffer (50 mM sodium acetate, 100 mM NaCl, pH 5) supplemented with a redox glutathione couple (10 mM reduced, 1 mM oxidised).

RodA was obtained from the fusion protein by cleavage with UBP41 and further purification by affinity chromatography and reverse-phase high-pressure liquid chromatography (HPLC). After the refolding step, the H_6-Ub-RodA containing samples were dialysed against the cleavage buffer (50 mM TrisHCl, 50 mM NaCl, 2 mM $CaCl_2$, pH 8) and incubated at 37°C for 2.5 h in the presence of the deubiquinating enzyme UBP41 (20:1 w:w protein:protease ratio). The UBP41 protease, which contains a hexa-histidine tag and cleaves at a specific C-terminal site on ubiquitin fusions, was previously prepared as described in (Kwan *et al.* 2006). H_6-ubiquitin, uncleaved H_6-Ub-RodA and the histidine-tagged UBP41 protease were removed by affinity chromatography on a nickel Hi-Trap™ column. The column was pre-equilibrated with 50 mM TrisHCl, 300 mM NaCl, 2 mM $CaCl_2$, 20 mM imidazole, pH 8. The cleaved mixture was loaded on the column after adjusting the NaCl and imidazole concentrations to 300 and 20 mM, respectively. RodA was eluted with the equilibrating buffer. A final HPLC purification step using a semi-preparative reverse phase C18 column (PepRPC 15 µm HR 10/10, Amersham Biosciences) was performed to separate the folded from the unfolded/partially folded forms of RodA, as well as to further purify the protein. The HPLC column was equilibrated with 10% methanol, 0.1% TFA. After adjusting the pH to *ca.* 4 with HCl, the RodA sample was loaded on the column and a linear gradient from 0 to 100% of acetonitrile (90 min) in equilibrating buffer was applied. Folded RodA-containing samples were pooled and lyophilised. Protein concentrations were determined by the bicinchoninic acid assay (BCA, Pierce Thermo Scientific) and/or absorption spectrophotometry, protein identity and integrity were monitored by SELDI-TOF (surface enhanced laser desorption/ionization time-of-flight) mass spectrometry and N-terminal microsequencing (Protein Analysis and Microsequencing Facility, Institut Pasteur), and purity was assessed by sodium-dodecyl-sulphate polyacrylamide gel electrophoresis under reducing conditions and NMR (^{15}N-^{1}H HSQC spectra). In addition, ^{15}N-^{1}H HSQC spectra served to establish the foldedness of the HPLC eluted fractions.

The recombinant protein obtained in this way consists of residues 19−159 of RodA and an additional N-terminal Ser residue that remains after cleavage of the fusion. The 18 N-terminal residues coded by the *RodA* gene, which correspond to the secretion signal and are expected to be cleaved by *A. fumigatus* upon secretion, were not cloned.

Doubly labelled RodA was also extracted by acid treatment from *A. fumigatus* spores obtained from minimal media containing ^{15}N NH_4Cl and $^{13}C_6$ glucose as described (Aimanianda *et al.* 2009) and purified by reverse-phase C18 HPLC as for the recombinant protein.

NMR spectroscopy

Doubly labelled (^{15}N, ^{13}C) recombinant RodA samples were prepared from lyophilised protein in 20 mM deuterated sodium acetate (CD_3COONa) buffer pH 4.3, 10% D_2O at a protein concentration of 0.36 mM.

NMR experiments were recorded on an Agilent DirectDrive 600 spectrometer (Agilent Technologies, Santa Clara) with a proton resonating frequency of 599.4 MHz. The spectrometer was equipped with a triple resonance cryogenic probe. Experiments were run at 25°C and referenced to internal sodium 4,4-dimethyl-4-silapentane-1-sulphonate following IUPAC recommendations. Data were collected using VnmrJ 3.2A (Agilent Technologies), processed with NMRPipe (Delaglio *et al.* 1995) and analysed with CCPNMR Analysis (Vranken *et al.* 2005).

Standard two- and three-dimensional experiments were recorded to assign chemical shifts to the protein ^{1}H, ^{13}C and ^{15}N nuclei. Backbone and CB resonances were assigned using [^{1}H-^{13}C/^{15}N] HSQC, HNCO, HNCACB, CBCA(CO)NH, HNCA and HNHA spectra. Side chains signals were assigned through H(CC-TOCSY)NNH, C(CC-TOCSY)NNH, HCCH-TOCSY, (HB)CB(CGCD)HD and (HB)CB(CGCDCE)HE experiments.

Typical spectral widths were 12.6 ppm for ^{1}H, 31.5 ppm for ^{15}N and 80 (aliphatic carbon), 14 (carbonyl), 30 (aromatic carbon), 36 (α carbon), or 22 ppm (β carbon) for ^{13}C spectral regions.

Assignments and secondary structure

Doubly labelled (^{15}N, ^{13}C) recombinant RodA was produced in *E. coli* as a fusion protein with His_6-tagged ubiquitin. The fusion protein was purified under denaturing conditions, refolded *in vitro* with a glutathione redox couple, cleaved and further purified by affinity chromatography and reverse-phase HPLC. ^{1}H-^{15}N HSQC spectra (Figure 1) showed a chemical shift dispersion typical of folded proteins.

The ^{1}H, ^{13}C and ^{15}N resonances of RodA were identified following a standard strategy (see Methods) that led to nearly complete assignments. Only side chain exchangeable groups from 4 Asn residues, 8 Lys and one Arg residue, some non-exchangeable side chain resonances (K33 Cδ, K111 $C\varepsilon H\varepsilon_2$, F23 Cδ, F85 Cε and $C\zeta H\zeta$) as well as 8 backbone carbonyls from residues preceding Pro residues and from the C-terminal residue, were not identified. All assigned chemical shifts have been deposited to the BMRB (accession code: 19782).

The redox state of the eight Cys residues of recombinant RodA was analysed using the Cys Cβ and Cα chemical shifts as described by Sharma and co-workers (Sharma and Rajarathnam 2000). The data is consistent with all the Cys residues being involved in disulphide bonds. Importantly, preliminary analysis of the pattern of ^{1}H-^{1}H nuclear Overhauser effects (nOes) observed in ^{13}C and ^{15}N edited NOESY spectra (not shown), unambiguously indicated that the disulphide bonds are formed by cysteines C1−C6 (39−116), C2−C5 (47−110), C3−C4 (48−88) and C7−C8 (117−135). The latter pattern is in accordance with the one established by chemical methods for other hydrophobins isolated from fungal sources (Kwan *et al.* 2006) or by X-ray crystallography from recombinant proteins (Hakanpaa *et al.* 2006a;Hakanpaa *et al.* 2006b), supporting that this pairing is a characteristic feature of hydrophobins. Furthermore, the superposition of ^{15}N-^{1}H HSQC spectra of the recombinant protein and the protein extracted from *A. fumigatus* spores (not shown) indicated that the recombinant and *A. fumigatus* proteins show the same structure and disulphide bond pattern. Therefore, the recombinant protein is natively folded and contains the native S−S bond topology.

The secondary structure of RodA was determined from the backbone and Cβ chemical shifts using the PECAN software (Eghbalnia *et al.* 2005). It consists of four β-strands (S1: Q44−T52, S2: L82−C88, S3: I114−C117, S4: L133−C135) and two α-helices (H1: V32−K38, H2: G63−L72). Except for helix H1, the secondary structure elements are located in the vicinity of cysteine residues (Figure 2A).

The dynamics of RodA on the nano-pico second time scale were analysed using the RCI method (Berjanskii and Wishart 2005). RCI values, which are a quantitative measure of how close the backbone and CB chemical shifts of a given residue are to their corresponding “random coil” values, are positively correlated with the amplitude of

motions on the nanosecond to picosecond time scale. Hence, the higher the RCI value, the higher the flexibility. The RCI values calculated for RodA indicated that the N-terminal region (S1−N19) is disordered and that the loops between cysteine residues C4−C5 and C7−C8, and to a lesser extent a region (N71−T79) of the long C3−C4 loop, are highly flexible (Figure 2B).

Comparison with other class I hydrophobins

The comparison of the secondary structure and dynamics (RCI values) of RodA, and the class I hydrophobins EAS from *Neurospora crassa* (Kwan *et al.* 2006), DewA from *Aspergillus nidulans* (Morris *et al.* 2011a;Morris *et al.* 2013) and MPG1 from M*agnaporthe oryzae* (Rey *et al.* 2013) is shown in Figure 2. The limited sequence similarity and varying length of these hydrophobins is translated into different secondary structures. Nevertheless, the proteins display common features centred on the four conserved disulphide bridges. Indeed, the four hydrophobins show β-strands in the vicinity of all the S−S bonds. This observation strongly suggests that the RodA (and MPG1) structure will show the characteristic β-barrel topology organised around the S−S bridges observed for EAS and DewA, as well as for the class II hydrophobins HFB1 and HFBII (Hakanpaa *et al.* 2006a;Hakanpaa *et al.* 2006b). Besides the β-barrel secondary structure, two common features can be highlighted for these class I hydrophobins. The first is a C7−C8 loop devoid of secondary structures and the second is, for hydrophobins with long N-terminal regions preceding the first cysteine (C1), a disordered N-terminal sequence of varying length (high RCI values, Figure 2B) followed by an α-helix close to the first disulphide bridge (C1−C6). In the case of DewA, the latter α-helix packs against the β-barrel and the alignment suggests that this might hold true for RodA and MPG1. The secondary structure content in other regions of the proteins, *i.e.* in the C3−C4 and C4−C5 regions, differs in the four proteins. In these regions, RodA shows two secondary structure elements that are not observed in EAS, DewA or MPG1: a long α-helix in the C3−C4 loop and a short α-helix in the C4−C5 loop. Regarding the nanosecond to picosecond dynamics, the RCI data indicates that the β-barrel region is rather rigid for the four proteins, while the C7−C8 and C3−C4 regions are flexible at least in some segment(s), except for DewA. The C4−C5 region of RodA also shows significant dynamics, a feature not observed in the corresponding region in other hydrophobins.

In summary, our data strongly suggest that RodA adopts the characteristic β-barrel topology observed in other hydrophobin structures, and indicates that it displays novel secondary structure elements, as well as a highly flexible N-terminal region and C4−C5 and C7−C8 loops. Interestingly, the highly flexible C7−C8 loop of EAS contains an amyloidogenic sequence (FLIIN) that has been shown by mutagenesis and peptide experiments to be implicated in the core cross β-structure of the EAS amyloid fibres (Macindoe *et al.* 2012). Flexibility of regions containing amyloidogenic sequences seems to be an important factor to allow the conformational changes that take place at the interface between hydrophobic and hydrophilic interfaces to form rodlets (Morris *et al.* 2011b). Amyloid prediction algorithms such as AMYLPRED (http://aias.biol.uoa.gr/AMYLPRED) predict an amyloidogenic sequence in the C7−C8 loop of RodA (data not shown). The assignments presented in this worked open the way for determining the structure of the soluble monomeric form of RodA, which will be valuable for the characterisation of the association mechanism into rodlets and for the study of RodA rodlets, which render the spores of the fungal pathogen *A. fumigatus* inert to the human immune system.

Acknowledgments

This work was funded by the ANR-10-Blanc SVSE 3-009 HYDROPHOBIN project, the European Community's Seventh Framework Programme [FP7/2007-2013] under Grant Agreement No: 260338 ALLFUN and the French-Australian Science & Technology (FAST) Program 2011. The 600 MHz spectrometer was funded by the Région Ile de France and the Institut Pasteur. We thank Jacques D'Alayer (Institut Pasteur) for initial SELDI-TOF and for N-terminal sequencing experiments.

Figure Captions

Fig. 1 $^{1}H-^{15}N$ HSQC spectrum of RodA. The spectrum was recorded at 25°C in buffer CD3COONa 20 mM, 10% D2O, pH 4.3. Assignments are shown only for backbone amide correlations. Chemical shifts (δ) are expressed in ppm relative to DSS (sodium 4,4-dimethyl-4-silapentane-1-sulphonate).

Fig. 2 (A) Sequence and secondary structure alignment of class I hydrophobins. Sequence alignment of class I hydrophobins with known structure and/or published chemical shifts was obtained by manual modification of a ClustalW alignment (Thompson *et al.* 1994) with constrained cysteine residue positions. Secondary structure was determined from backbone (N, C, Cα, Hα) and Cβ chemical shifts using the PECAN software (RodA and MPG1) or from structural ensembles (DewA and EAS) by means of the DSSP algorithm. α-helices are represented by cylinders and β-strands by arrows. Positions of Cys residues are numbered from 1 to 8 and are highlighted by horizontal green lines, while the disulphide topology is indicated by horizontal green lines. **(B)** Random coil index (RCI) as a function of alignment position. RCI values were calculated from chemical shifts deposited at the BMRB or in the case of EAS with unpublished chemical shifts, using the RCI software (Berjanskii and Wishart 2005). The RCI of the N-terminal residues of RodA and MPG1 are truncated for visualisation purposes. Secondary structure and Cys positions are displayed as in (A). In (B), blank spaces represent gap positions in the sequence alignment. Alignment position for RodA starts at residue 2, *i.e.*, at the first residue belonging to RodA in the recombinant protein used in this work.

Bibliography

1. Kwan AH, Winefield RD, Sunde M, Matthews JM, Haverkamp RG, Templeton MD, Mackay JP (2006) Structural basis for rodlet assembly in fungal hydrophobins. Proc Natl Acad Sci U S A 103: 3621-3626.
2. Wosten HA, Asgeirsdottir SA, Krook JH, Drenth JH, Wessels JG (1994) The fungal hydrophobin Sc3p self-assembles at the surface of aerial hyphae as a protein membrane constituting the hydrophobic rodlet layer. Eur J Cell Biol 63: 122-129.
3. Wosten HA, de Vocht ML (2000) Hydrophobins, the fungal coat unravelled. Biochim Biophys Acta 1469: 79-86.
4. Szilvay GR, Paananen A, Laurikainen K, Vuorimaa E, Lemmetyinen H, Peltonen J, Linder MB (2007) Self-assembled hydrophobin protein films at the air-water interface: structural analysis and molecular engineering. Biochemistry 46: 2345-2354.

5. Ren Q, Kwan AH, Sunde M (2013a) Solution structure and interface-driven self-assembly of NC2, a new member of the Class II hydrophobin proteins. Proteins.
6. Sunde M, Kwan AH, Templeton MD, Beever RE, Mackay JP (2008) Structural analysis of hydrophobins. Micron 39: 773-784.
7. Wosten HA (2001) Hydrophobins: multipurpose proteins. Annu Rev Microbiol 55: 625-646.
8. Scholtmeijer K, Wessels JG, Wosten HA (2001) Fungal hydrophobins in medical and technical applications. Appl Microbiol Biotechnol 56: 1-8.
9. Tucker SL, Talbot NJ (2001) Surface attachment and pre-penetration stage development by plant pathogenic fungi. Annu Rev Phytopathol 39: 385-417.
10. Linder MB, Szilvay GR, Nakari-Setala T, Penttila ME (2005) Hydrophobins: the protein-amphiphiles of filamentous fungi. FEMS Microbiol Rev 29: 877-896.
11. Bayry J, Aimanianda V, Guijarro JI, Sunde M, Latge JP (2012) Hydrophobins--unique fungal proteins. PLoS Pathog 8: e1002700.
12. Ren Q, Kwan AH, Sunde M (2013b) Two forms and two faces, multiple states and multiple uses: Properties and applications of the self-assembling fungal hydrophobins. Biopolymers 100: 601-612.
13. Hayes GE, Denning DW (2013) Frequency, diagnosis and management of fungal respiratory infections. Curr Opin Pulm Med 19: 259-265.
14. Paris S, Debeaupuis JP, Crameri R, Carey M, Charles F, Prevost MC, Schmitt C, Philippe B, Latge JP (2003) Conidial hydrophobins of Aspergillus fumigatus. Appl Environ Microbiol 69: 1581-1588.
15. Aimanianda V, Bayry J, Bozza S, Kniemeyer O, Perruccio K, Elluru SR, Clavaud C, Paris S, Brakhage AA, Kaveri SV, et al. (2009) Surface hydrophobin prevents immune recognition of airborne fungal spores. Nature 460: 1117-1121.
16. Delaglio F, Grzesiek S, Vuister GW, Zhu G, Pfeifer J, Bax A (1995) NMRPipe: a multidimensional spectral processing system based on UNIX pipes. J Biomol NMR 6: 277-293.
17. Vranken WF, Boucher W, Stevens TJ, Fogh RH, Pajon A, Llinas M, Ulrich EL, Markley JL, Ionides J, Laue ED (2005) The CCPN data model for NMR spectroscopy: development of a software pipeline. Proteins 59: 687-696.
18. Sharma D, Rajarathnam K (2000) 13C NMR chemical shifts can predict disulfide bond formation. J Biomol NMR 18: 165-171.
19. Hakanpaa J, Linder M, Popov A, Schmidt A, Rouvinen J (2006a) Hydrophobin HFBII in detail: ultrahigh-resolution structure at 0.75 A. Acta Crystallogr D Biol Crystallogr 62: 356-367.
20. Hakanpaa J, Szilvay GR, Kaljunen H, Maksimainen M, Linder M, Rouvinen J (2006b) Two crystal structures of Trichoderma reesei hydrophobin HFBI--the structure of a protein amphiphile with and without detergent interaction. Protein Sci 15: 2129-2140.
21. Eghbalnia HR, Wang L, Bahrami A, Assadi A, Markley JL (2005) Protein energetic conformational analysis from NMR chemical shifts (PECAN) and its use in determining secondary structural elements. J Biomol NMR 32: 71-81.
22. Berjanskii MV, Wishart DS (2005) A simple method to predict protein flexibility using secondary chemical shifts. J Am Chem Soc 127: 14970-14971.
23. Morris VK, Kwan AH, Mackay JP, Sunde M (2012) Backbone and sidechain (1)H, (13)C and (15)N chemical shift assignments of the hydrophobin DewA from Aspergillus nidulans. Biomol NMR Assign 6: 83-86
24. Morris VK, Kwan AH, Sunde M (2013) Analysis of the structure and conformational states of DewA gives insight into the assembly of the fungal hydrophobins. J Mol Biol 425: 244-256.
25. Rey AA, Hocher A, Kwan AH, Sunde M (2013) Backbone and sidechain (1)H, (13)C and (15)N chemical shift assignments of the hydrophobin MPG1 from the rice blast fungus Magnaporthe oryzae. Biomol NMR Assign 7: 109-112.
26. Macindoe I, Kwan AH, Ren Q, Morris VK, Yang W, Mackay JP, Sunde M (2012) Self-assembly of functional, amphipathic amyloid monolayers by the fungal hydrophobin EAS. Proc Natl Acad Sci U S A 109:E804-811.
27. Morris VK, Ren Q, Macindoe I, Kwan AH, Byrne N, Sunde M (2011b) Recruitment of Class I Hydrophobins to the Air:Water Interface Initiates a Multi-step Process of Functional Amyloid Formation. J Biol Chem 286: 15955-15963.
28. Thompson JD, Higgins DG, Gibson TJ (1994) CLUSTAL W: improving the sensitivity of progressive multiple sequence alignment through sequence weighting, positions-specific gap penalties and weight matrix choice. Nucleic Acids Res 22: 4673-4680.

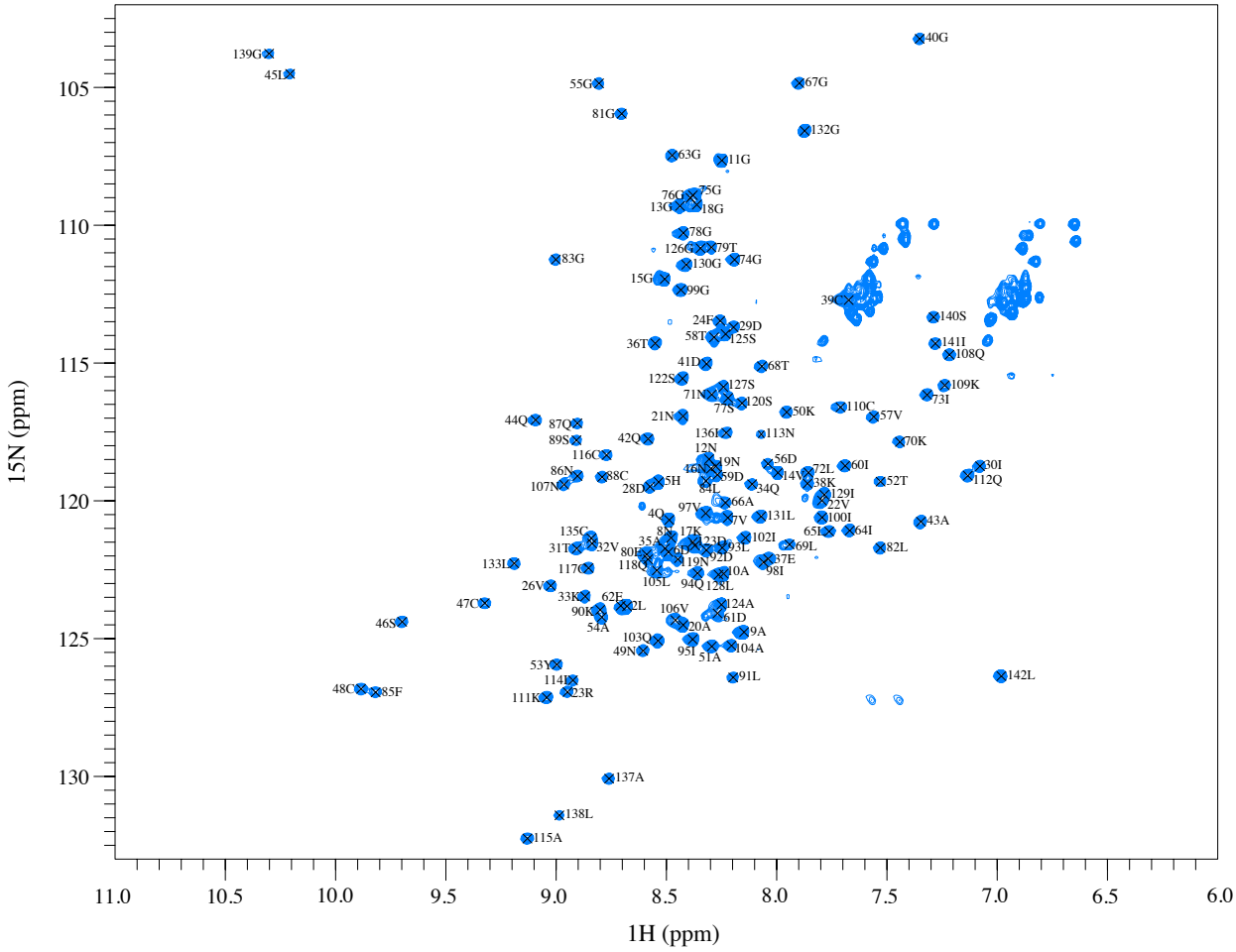
15N (ppm)
1H (ppm)
105
110
115
120
125
130
11.0
10.5
10.0
9.5
9.0
8.5
8.0
7.5
7.0
6.5
6.0
139G
45L
55G
81G
40G
67G
132G
63G
11G
75G
76G
13G
18G
78G
126G
79T
83G
130G
74G
15G
99G
24F
29D
58T
125S
36T
140S
141I
108Q
41D
68T
122S
127S
109K
73I
71N
77S
120S
50K
110C
57V
44Q
87Q
21N
89S
42Q
136I
113N
70K
12N
116C
56D
60I
30I
86N
88C
59D
72L
112Q
107N
28D
5H
84L
34Q
38K
52T
129I
22V
4Q
97V
66A
43A
135C
17K
131L
100I
102I
65I
64I
31T
32V
69L
82L
133L
117C
118C
19N
92D
87E
10A
98I
105L
94Q
128L
26V
33K
62E
2L
106V
124A
47C
90L
61D
46S
54A
20A
9A
103Q
49N
95I
51A
104A
53V
114I
91L
142L
48C
85F
111K
23R
137A
138L
115A

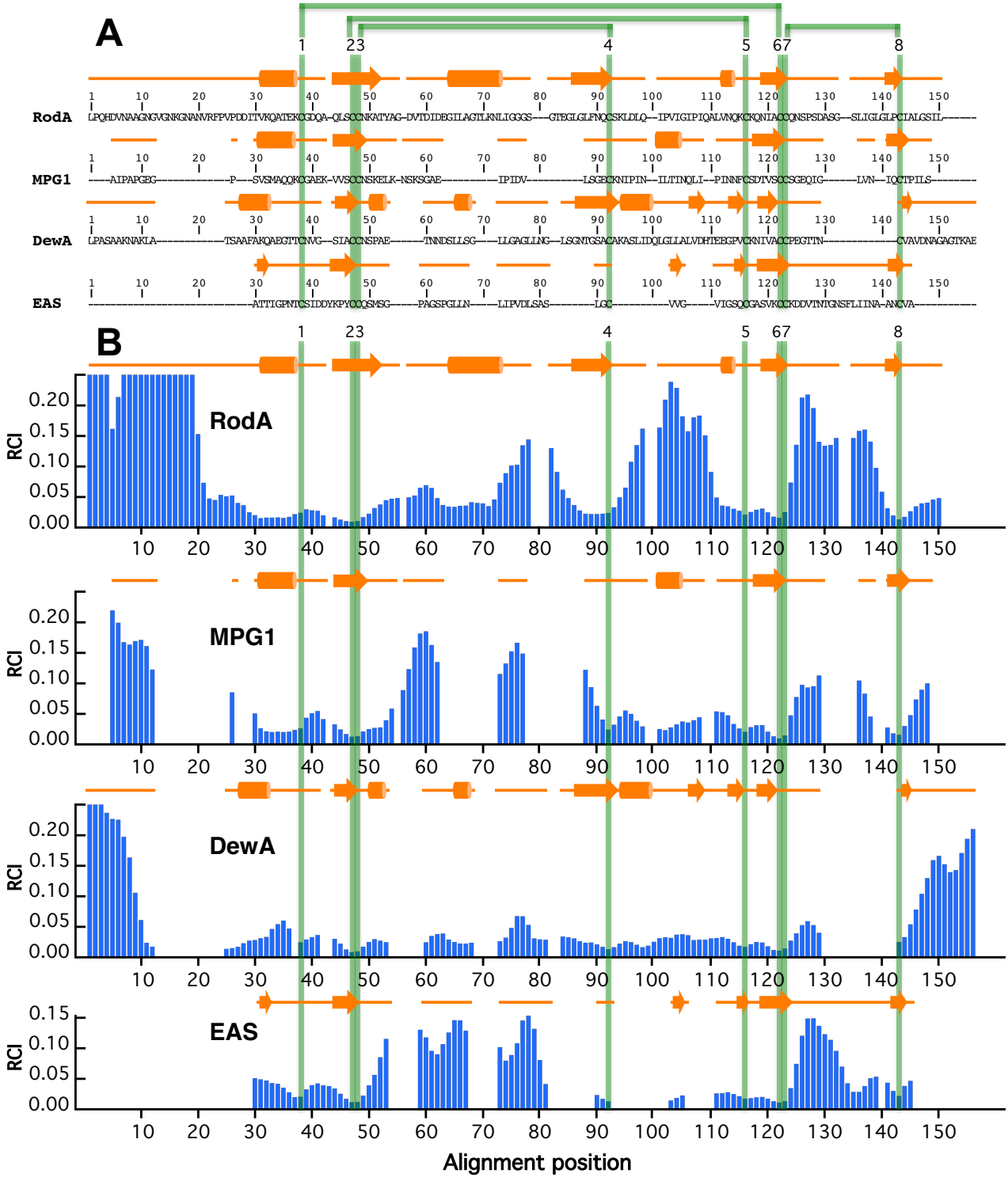
A
1
23
4
5
67
8
RodA
MPG1
DewA
EAS
B
RodA
MPG1
DewA
EAS
RCI
0.20
0.15
0.10
0.05
0.00
10
20
30
40
50
60
70
80
90
100
110
120
130
140
150
Alignment position